

Geometry dependence of heating in a U-tube heat exchanger for pasteurization

Jerry James M. de la Torre^{1*}, Alvin B. Culaba², Romualdo C. Martinez¹

(1. *Philippine Center for Postharvest Development and Mechanization, Nueva Ecija, Philippines;*

2. *Mechanical Engineering Department, De La Salle University, Manila, Philippines)*

Abstract: A serpentine tube heat exchanger is physically constrained by its bend radius. The U-tube bend section of a tubular heat exchanger is thus interesting broadly in terms of fluid flow and heat transfer. This paper presents the tube size dependence of heating profile of this U-tube as is commonly encountered in the design of pasteurizers. Analytical and computational modeling were employed in investigating the heat capacity, heat flux, heating rate and energy use of a U-tube at increasing diameters 9.52, 12.70, 19.05 and 25.40 mm, each at constant 1 mm thickness. SolidWorks 2016 was used in geometric modeling while Ansys v16 was used for transient thermal computational fluid dynamics simulation of the conduit (SS316L) and the product (coconut water). The initial conditions were $5,000 \text{ W m}^{-2} \text{ K}^{-1}$ convective heat supply at 95°C and 92°C surface temperature for the conduit and the product, respectively. Both the tube and the product were initially at 30°C. The tube, whose heating profile was independent of size, reached 90°C in 2.1 s. For the product, as the tube size increases, the heat capacity increases exponentially ($Q_p = 108.3e^{0.1831x}$), the heat flux drops down 57% within 40 s, while both the heating rate ($T_{t=60s} = -48\ln(x) + 183.65$) and the energy use ($Q_u = -29.65\ln(x) + 235.36$) drops logarithmically. These results are beneficial to designers and engineers in sizing of heaters, minimizing fouling and optimizing energy efficiency as well as pasteurizer processing capacity.

Keywords: Tubular heat exchanger, heat transfer, modeling and simulation, pasteurizer, coconut water

Citation: de la Torre, J. J. M., A. B. Culaba and R. C. Martinez. 2021. Geometry dependence of heating in a U-tube heat exchanger for pasteurization. *Agricultural Engineering International: CIGR Journal*, 23(3):238-250.

1 Introduction

Pasteurization is conventionally a thermal process by nature where the spoilage constituents in a liquid food are subjected to heating for a certain time to kill or inactivate them, thereby preserving the food quality for a longer

period (University of Guelph, 2020). At the core of this thermal treatment therefore is the heat exchanger, which may come in varying forms. The geometry dependence of heat and mass transfer is specifically important in determining heat load, calculating rate of heating, sizing the heater, estimating thermal gradient and cold spots, heat recovery, fouling, variable loading and optimizing pasteurizer processing capacity (Aguiar and Gut, 2014; Gutierrez et al., 2014; Kic and Zajicek, 2015; Narataruksa et al., 2010; Negiz et al., 1998; Petermeier et al., 2002).

One configuration of a tube heat exchanger includes a U-shaped bend to compress a rather very long product conduit in a more compact volume. In this paper, this U-

Received date: 2020-05-14 **Accepted date:** 2020-11-09

* **Corresponding author:** Jerry James M. de la Torre, Bioprocess Engineering Division, Philippine Center for Postharvest Development and Mechanization (PHilMech), CLSU Compound, Munoz Science City, Nueva Ecija, 3120, Philippines. Email: jerry_delatorre@dlsu.edu.ph, Tel. 63.44.456 0287, Fax: 63.44.456 0110.

tube segment was taken as a focus of interest because of its significance not only in heat transfer but also in fluid flow and manufacturing aspects. In terms of fluid flow, it has been established that bends naturally disrupt velocity profiles, thereby affecting transport mechanisms (Guan and Martonen, 1997). From the manufacturing aspect, it has been considered an industry standard that the minimum bend radius of this U-tube is twice the tube diameter (Listertube, 2020). These physical constraints serve as compelling considerations why the U-tube segment is taken as an object of heat transfer analysis. In pasteurization, it is desirable to heat up the product as fast as possible while minimizing thermal gradient as well as avoiding internal tube surface burning which may lead to fouling. It has been observed that constituents in liquid food such as proteins in milk, sugars and pulp particulates in juice may get burned and deposited in the heat exchanger conduit leading to reduced heat transfer over time. It was also noted that these deposits accumulate faster in sections of slower flow (Berk, 2013). A U-tube is an example of these sections.

Currently, the high temperature short time (HTST) pasteurization process is generally favored for its greater benefit in preserving food quality while destroying the undesirable constituents (Petruzzi et al., 2017). However, there are limited papers on modeling the heat transfer aspect of HTST process as a function of geometry of the heat exchanger (Jha et al., 2019).

In a modeling study of a tubular heat exchanger, the geometry design was considered but the approach was an initial arbitrary choice of diameter, then solving for the required heat transfer area to finally determine the length of the tube (Bonafoni and Capata, 2015). Unlike that study, this paper attempts to establish heat transfer implications in a U-tube at varying radii, and considering bend radius is dependent on tube diameter, the tube length and volume change accordingly each time.

2 Methodology

This study was conducted on January to May, 2020 at De La Salle University (DLSU), Manila, Philippines and the Philippine Center for Postharvest Development and Mechanization (PHilMech), Nueva Ecija, Philippines as part of a bigger ongoing research project on the design and development of an intelligent pasteurizer for coconut water.

The heating system is a shell and tube heat exchanger (Barbosa-Canovas and Ibarz, 2003) as represented by the schematic model below (Figure 1) where the main heat supply Q_s comes from a boiler line into one side of the shell heat exchanger, then coming out of the other side, in a recirculating fashion. The notation i and o refers to inflow and outflow, respectively. The product flows inside a bundle of small tubes and these tubes are fully exposed to the heating fluid on all the external surface such that the heat is transferred initially by convection, then by conduction through the tube and the heat is then absorbed by the product by convection. The product heat load is denoted by Q_p while the heat loss to the environment through the shell wall is indicated as Q_L . The heat absorbed by both the conduit and the product is designated as Q_A .

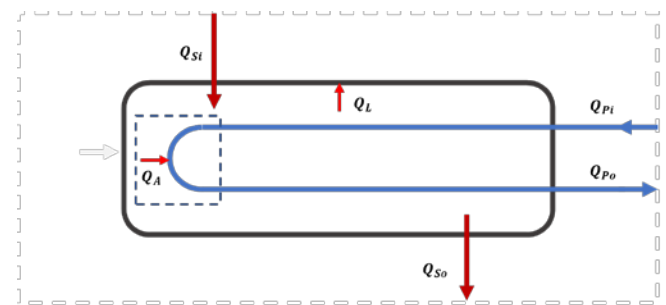


Figure 1 Shell and tube heating system of the pasteurizer

The object of investigation of this paper is confined to the heat transfer in the U-tube bend of the product conduit as shown enclosed in the dashed square (Figure 1). As such, the model can be simplified in a localized model as shown below (Figure 2) where the heat notation was changed from global Q to a more specific q .

The energy balance from the domain of heat transfer analysis is given in the subsequent equations below. The net energy expenditure ($q_{Si} - q_{So}$) of the heating region is dissipated into the main heat load q_A (heat capacity of

the tube and the heating requirement of the liquid product) as well as the heat loss q_L towards the wall of the shell of the heat exchanger.

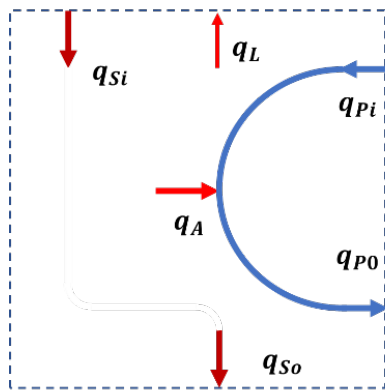


Figure 2 Domain of heat transfer analysis

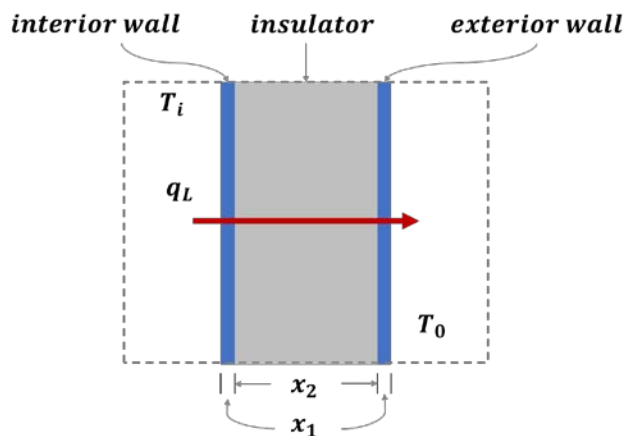


Figure 3 Model of heat loss q_L through the cross section of the shell of the heat exchanger

$$q_{Si} = q_{So} + q_A + q_L \quad (1)$$

where:

q_{Si} = incoming heat supply, kJ

q_{So} = energy of the outgoing fluid, kJ

q_A

= energy absorbed by both the tube and the product, kJ

q_L = heat loss at the wall of the heat exchanger, kJ

The heat requirement of the product ($q_{Po} - q_{Pi}$) is the magnitude of energy required to raise its temperature to the desired pasteurization level from its raw state. The heat loss q_L is deemed negligible under the following conditions: a) the heat exchanger has a sufficiently large shell relative to the bundle of product tubes; b) the boiler is big enough to heat a large mass of heating fluid

recirculating around the bundle of product tubes, and c) the shell is adequately insulated.

The heat loss q_L through the composite wall is represented by the model below (Figure 3) where q_L has to pass through the interior wall (thickness x_1), insulator (thickness x_2) and out into the open environment through the exterior wall (thickness x_1) at a lower ambient temperature T_0 from the heated interior temperature T_i .

Considering a cross-section slab of the shell heat exchanger with a unit area $A = 1 \text{ m}^2$, with an insulator ($k = 0.026 \text{ W} \cdot \text{m}^{-1} \cdot \text{°C}^{-1}$, $x_2 = 50 \text{ mm}$) made of polyurethane material (Shawyer and Pizzali, 2003) between a wall (SS304, $x_1 = 1.2 \text{ mm}$) of identical stainless steel (The World Material, 2020), the heat loss q_L through this composite wall is merely 0.68% of the convective flux from the heating fluid at interior temperature $T_i = 95\text{°C}$ and exterior temperature $T_0 = 30\text{°C}$. This is practically a steady state heat transfer through a multilayer slab (Barbosa-Canovas and Ibarz, 2003; Berk, 2013). By this calculation, q_L can be treated negligible.

The design approach of this paper is inductive, going from local to global requirements. Hence, the optimal product flow, bundle of tubes, the shell geometry, insulation, boiler specifications and the system interaction of these elements will be treated in another paper.

2.1 Geometric modeling of a U-tube heat exchanger

The U-tube section (Figure 4) of the tubular heat exchanger was drawn in three dimensional visual model using Solidworks (Dassault Systèmes SolidWorks Corporation, 2020) version 2016 for tube diameters, $d = 9.52, 12.70, 19.05$ and 25.40 mm , which are more commonly known in the Philippines in their English units, $d = 3/8, 1/2, 3/4$ and 1 in . The bend radius, R , was held at $R = 2d$, in accordance with industry standard minimum bend. The thickness was kept constant at 1 mm .

For the subsequent computational modeling and simulation, the geometry objects at various tube sizes were exported as an IGS file.

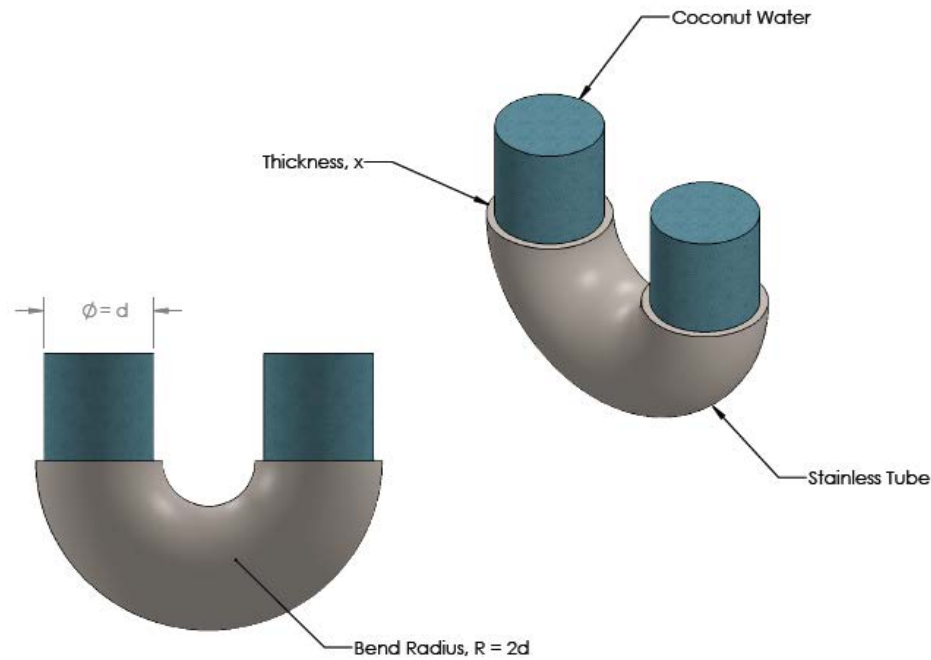


Figure 4 Objects of heat transfer modeling: U-tube section of a heat exchanger in a pasteurizer and the coconut water product

2.2 Kinematic modeling: heat capacity

Based from the fundamental heat transport in Equation 2 (Welti-Chanes et al., 2005), the heat capacity calculations for the conduit and the product as constrained by the U-tube geometry were derived in Equations 3 and 4 below.

$$\text{Heat Capacity, } Q, J \quad Q = \int_{T_i}^{T_f} m C_p dT \quad (2)$$

where:

$$m = \text{mass, } g$$

$$C_p = \text{specific heat of the material, } J \cdot g^{-1} \cdot ^\circ C^{-1}$$

dT = change in temperature,

T , initially from T_i to endpoint T_f , $^\circ C$

Heat Capacity of the product, Q_p, J

$$Q_p = 2\pi^2 \int_{T_i}^{T_f} \rho_p C_p r^3 dT \quad (3)$$

where:

$$\rho_p = \text{density of the product, } g/cm^3$$

$$C_p = \text{specific heat of the product, } J \cdot g^{-1} \cdot ^\circ C^{-1}$$

r = radius of the tube, cm

dT = change in temperature initially

from T_i to endpoint T_f , $^\circ C$

Heat Capacity of the conduit tube, Q_t, J

$$Q_t = 4\pi^2 \int_{T_i}^{T_f} \rho_t C_t r^2 x dT \quad (4)$$

where:

$$\rho_t = \text{density of the product, } g/cm^3$$

$$C_t = \text{specific heat of the product, } J \cdot g^{-1} \cdot ^\circ C^{-1}$$

r = radius of the tube, cm

x = thickness of the tube, cm

dT = change in temperature initially

from T_i to endpoint T_f , $^\circ C$

The heat capacity calculations were based on the subsequent material assignments and properties, as indicated in Table 1 below.

2.3 Computational modeling and simulation: heat flux and thermal gradient

The heat flux and thermal gradient were computed and visualized using transient thermal modeling and simulation in Ansys v16. The geometry and material properties from the previous section were applied. In meshing, the following settings were made: coarse sizing at reference center; medium smoothing; fast transition; program

controlled triangle surface mesh; 2,273 to 2,910 to nodes, size. and 440 to 594 elements for the smallest to the biggest tube

Table 1 Material Properties

Properties	Unit	Value	Reference
<i>Coconut Water</i>			(Fontan et al., 2007)
Density, ρ	g/cm^3	1.0132	
Specific heat, C_p s	$J \cdot g^{-1} \cdot ^\circ C^{-1}$	4.0565	
Convective heat transfer coefficient, h_c	$W \cdot m^{-2} \cdot K^{-1}$	5,000	
Stainless Steel Tube, SS304			(The World Material, 2020)
Density, ρ	g/cm^3	7.93	
Specific heat, C_p s	$J \cdot g^{-1} \cdot ^\circ C^{-1}$	0.502	
Thermal conductivity, k	$W \cdot m^{-1} \cdot ^\circ C^{-1}$	12.6	

The boundary conditions are given as follows. The initial temperature for both the product and the conduit was 30°C. The convective heat supply was $5,000 W \cdot m^{-2} \cdot K^{-1}$, as is commonly applied in pasteurizers (Mathisson, 2015). The external surface of the conduit was exposed to this convective stream at 95°C. The product heating profile, on the other hand, was investigated when this convective load raises the internal tube surface temperature to 92°C, as in the case of an electric heater keeping the heating fluid practically stable on a certain duty cycle. The computational run time was extended until stable heating was achieved for all tube sizes. The product is considered at steady heating when the temperature converges to at least 90°C. This time was designated as flat heating time, $t_{T=90^\circ C}$. While at this, both heat flux and thermal gradient were noted for the first 60 s of the simulation. The minimum temperature at 60 s was defined as minute temperature and was assigned $T_{t=60 s}$. Both t_T and T_t are indicative benchmark figures in the subsequent heating rates adjustments.

2.4 Heat transfer analysis

The tube geometry and heat transfer analysis were evaluated in terms of heat load, heating rate, and energy use.

The heat load aspect pertains to the magnitude of heat capacity of the product, the conduit and the two objects added together. As such heat capacity ratio was computed at varying tube sizes, using the equation below.

Heat Capacity Ratio, Q_r

$$Q_r = \frac{\rho_p C_p r}{2 \rho_t C_t x} \quad (5)$$

where:

ρ_p = density of the product, g/cm^3

C_p = specific heat of the product, $J \cdot g^{-1} \cdot ^\circ C^{-1}$

r = radius of the tube, cm

ρ_t = density of the conduit tube, g/cm^3

C_t = specific heat of the tube, $J \cdot g^{-1} \cdot ^\circ C^{-1}$

x = thickness of the tube, cm

The heating rate was evaluated in a number of ways, such as the flat heating time, minute temperature and thermal gradient. All these three parameters were obtained from the transient thermal simulation at constant convective heat load at various tube sizes.

Energy use, Q_u , is simply the amount of energy expended to heat the product to a certain temperature. It was computed from the equation below.

$$\text{Energy Use, } Q_u, \text{ kJ/ml } Q_u = \frac{Q_T}{V_p} \quad (6)$$

where,

Q_T = Total heating energy, kJ

V_p = Product volume, ml

In a lossless model, the total heating energy is the sum of the heat capacity of the conduit and the product.

3 Results and discussion

3.1 Heat capacity

The heat capacity of the conduit (stainless steel tube) and the product (coconut water) at varying tube sizes is given in Figure 5 below.

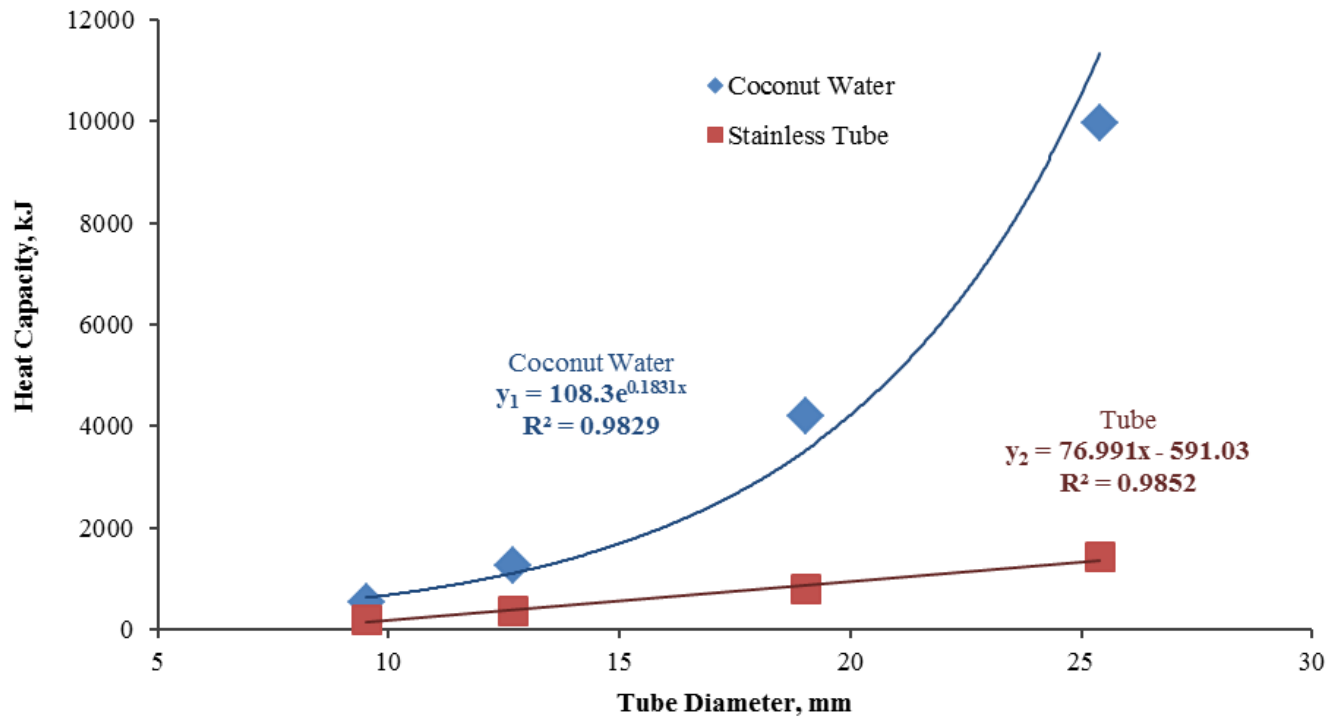
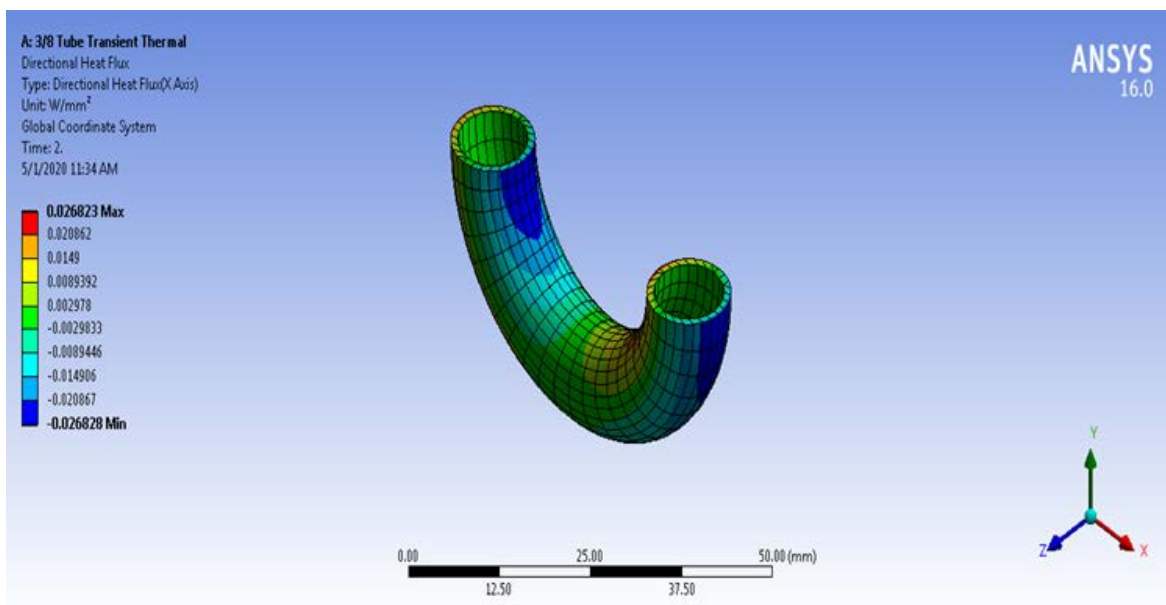


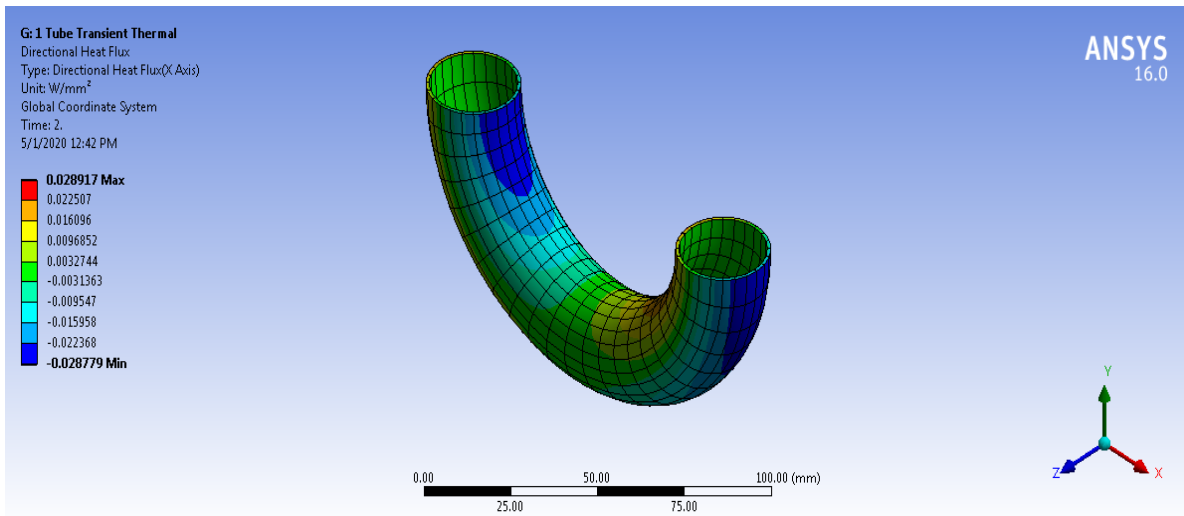
Figure 5 Heat capacity of the conduit and the product at varying tube sizes

As the tube diameter increases linearly by 2.67x, from 9.52 to 25.40 mm (3/8 to 1 in), the product heat load rises exponentially. The heat load at the biggest diameter (25.40 mm) is about 19x of the smallest tube (9.52 mm). It should be noted that as the tube diameter, x , increases, so does the volume, such that the surface to volume ratio, y , decreases

according to $y = -0.0892x + 0.4987, R^2 = 0.98$. Meaning, the volume increases much faster than the surface area. The volume practically serves as the heat sink while the surface area is the port of heat transfer. Given enough time, the product will absorb heat to its capacity.

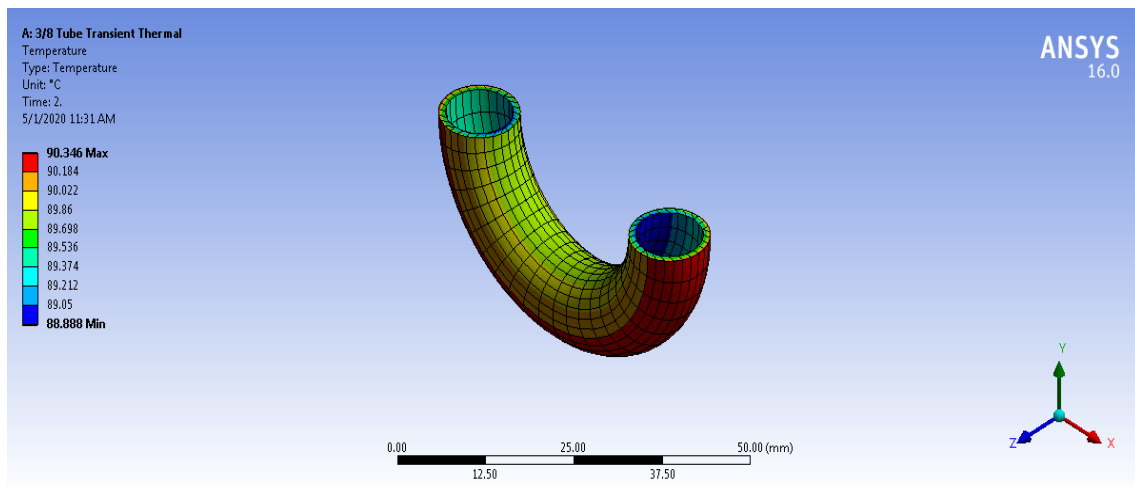


(a) the smallest tube

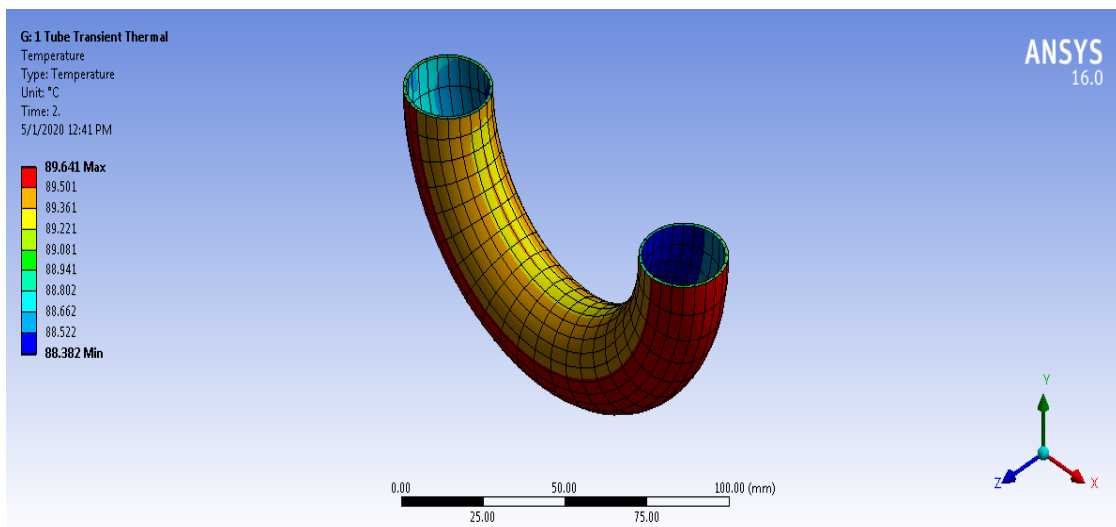


(b) the biggest tube

Figure 6 Heat flux for different tubes

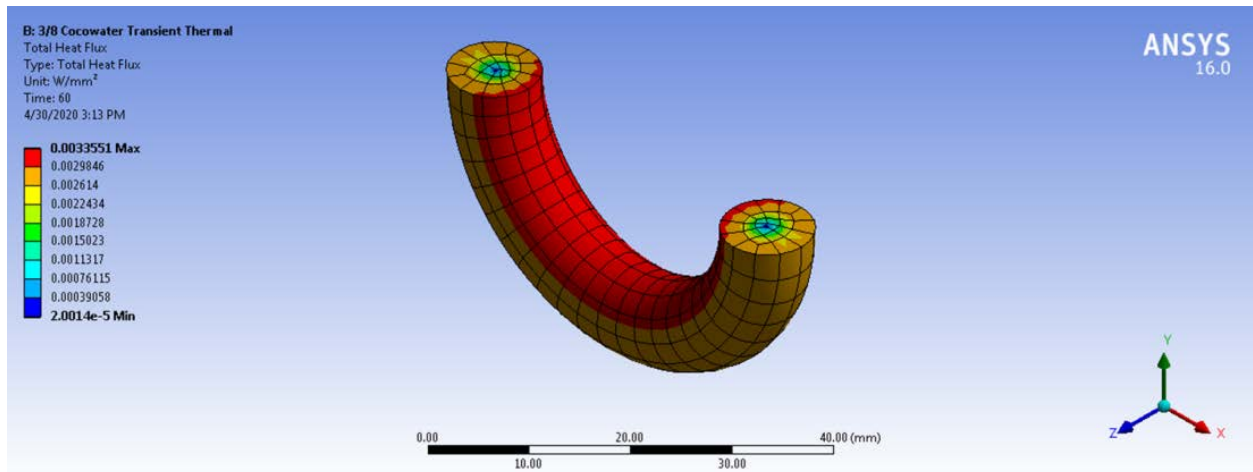


(a) The lower tube

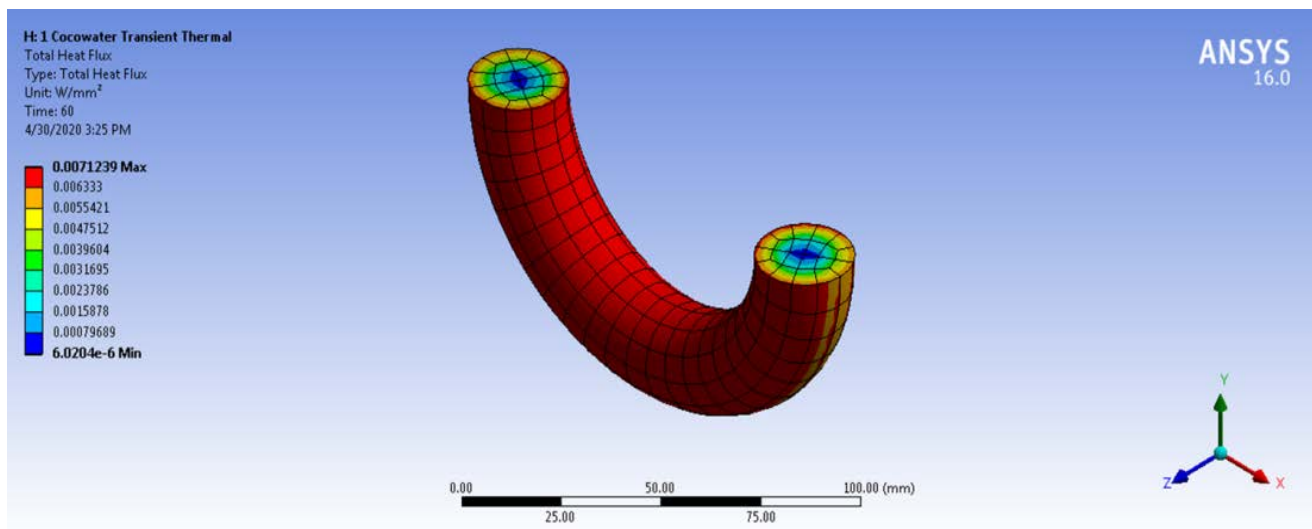


(b) The bigger tube

Figure 7 Thermal gradient for different tube



(a) The smallest tube



(b) The biggest tube

Figure 8 Heat flux for different tube

On the other hand, the thermal gradient is shown in Figure 7 below for the lower and bigger tube. Again, the intermediate simulation results were omitted for brevity. As the tube temperature rises to steady state, it follows the growth curve $y = 16.99 \ln(x) + 33.588$, $R^2 = 0.9609$, where y is the temperature in $^{\circ}\text{C}$. This is true for all tube sizes. To reach 90°C , it took only 2.1 s. This is very fast heating relative to the product. The product in the smallest tube and biggest tube requires 2.1 and 16.1 min, respectively, to reach 90°C . Simply put, the conduit tube heats up about 60 to 460 times faster than the product. This is an important concern in thermally gradient-induced deposit build-up in conduits. Knowing this, a suitable

design adjustment, like heat supply calibration or fluid flow regulation, can be made.

The heat flux for the product showed a convergence towards $2.85 \times 10^{-3} \text{ W/mm}^2$ at around 40 s which is about 57% of the initial convective heat load. Figure 8 below shows the heat flux gradient for the smallest and the biggest tube.

The minute temperature and thermal gradient are shown below for the smallest tube (Figure 9a) and the biggest tube (Figure 9b). The visualization for intermediate tube sizes were omitted for brevity of this report.

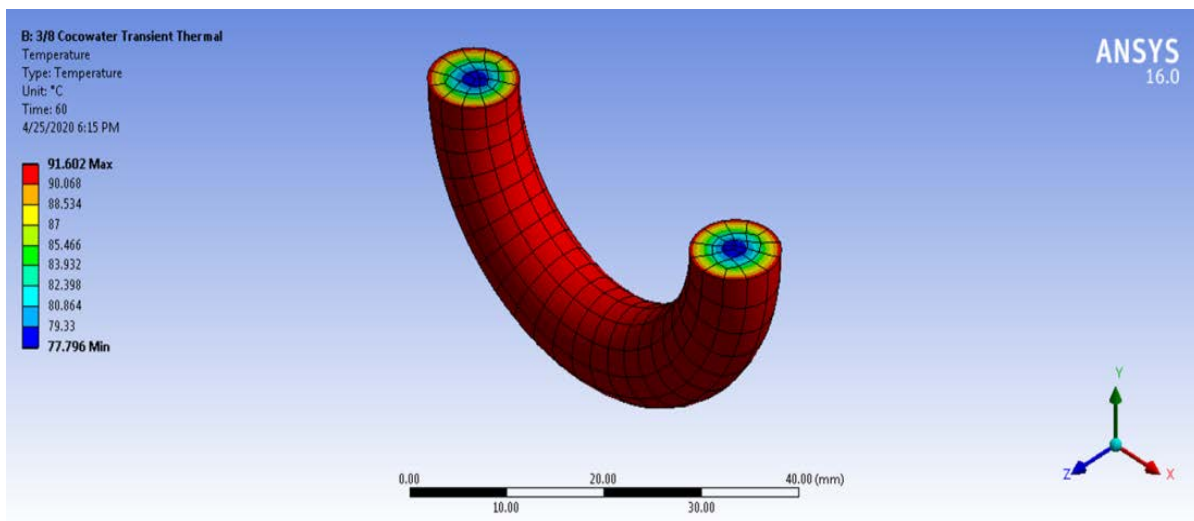
For the smaller tube (9.52 mm \varnothing), the temperature of the product rose to 77.6°C in 1

minute, initially from 30°C. This was equivalent to 47.6°C step. On the other hand, the biggest tube size (25.40 mm Ø) increased its temperature by merely 1.64°C, initially from 30°C. This means that given the same convective head load, the product got barely heated when the diameter was increased by 2.67×.

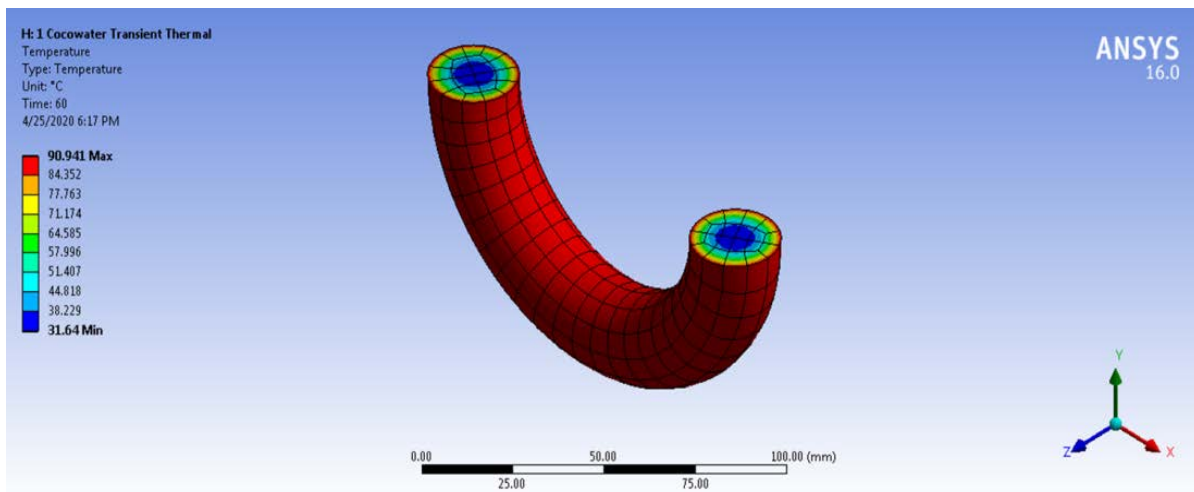
3.3 Heat transfer analysis

As the tube size increases, the heat capacity

ratio of the product and the conduit increases linearly from 2.64 to 7.03 (Figure 10). This increase is primarily due to the much faster increase by volume of the product than the volume of the conduit. This means further that as the tube size increases, the specific heat of the product becomes more of a significant factor to the magnitude of heat load, than the thermal property of the conduit.



(a) Lower tube, 3/8 in dia



(b) Bigger tube, 1 in dia

Figure 9 Minute temperature and thermal gradient at constant convective heat load for different tube

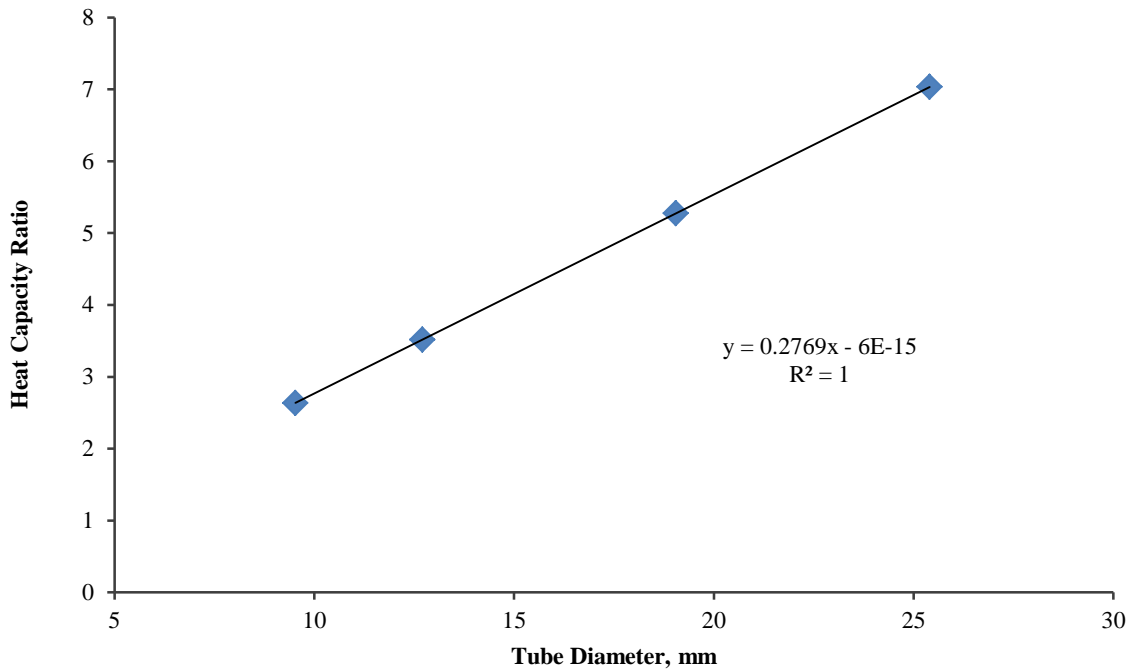


Figure 10 Heat capacity ratio of the product and the conduit as the tube diameter increases

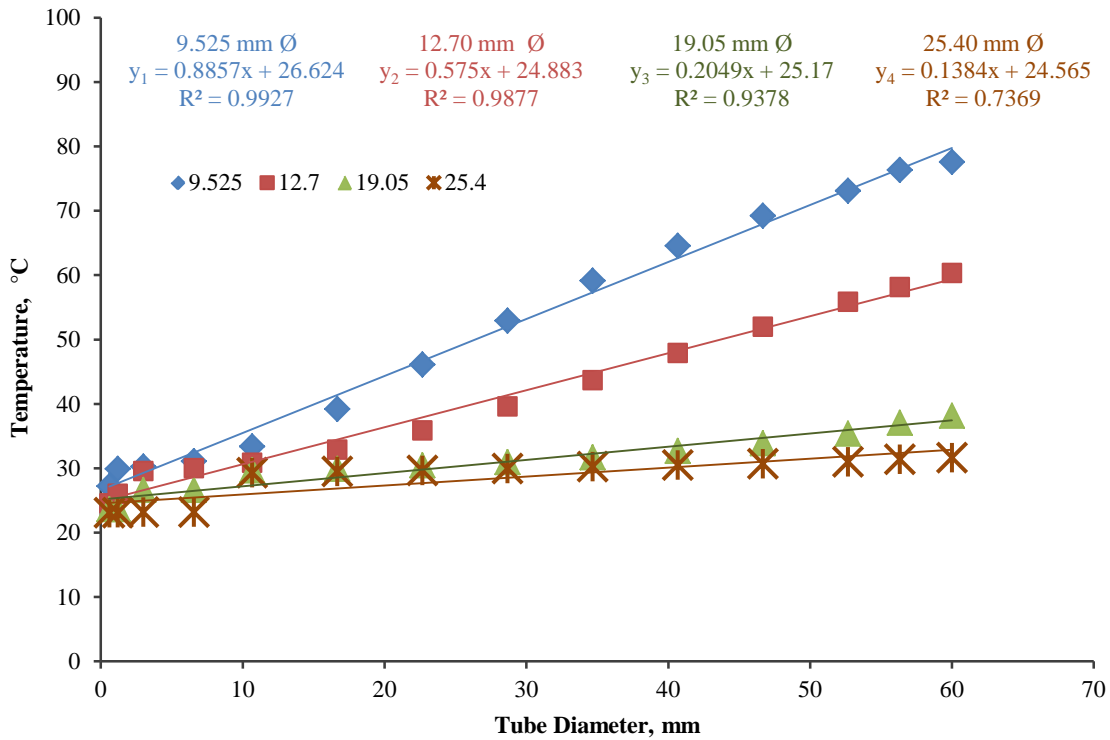


Figure 11 Minute temperature and thermal gradient at constant convective heat load for varying tube sizes

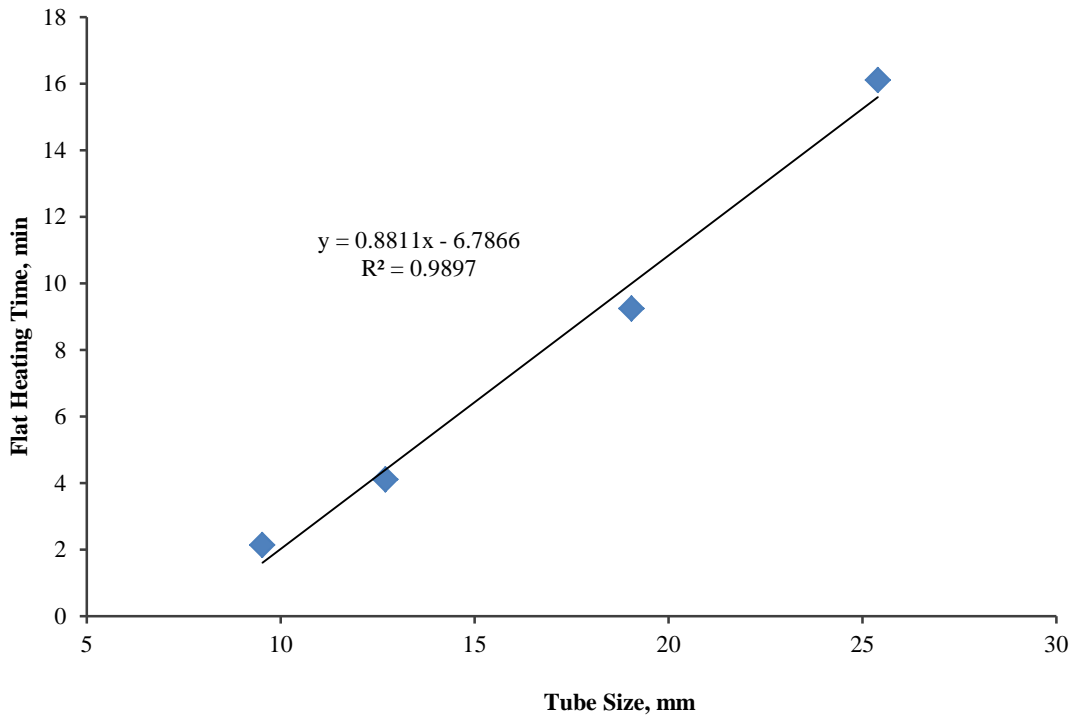


Figure 12 Flat heating time at constant convective heat load for varying tube sizes

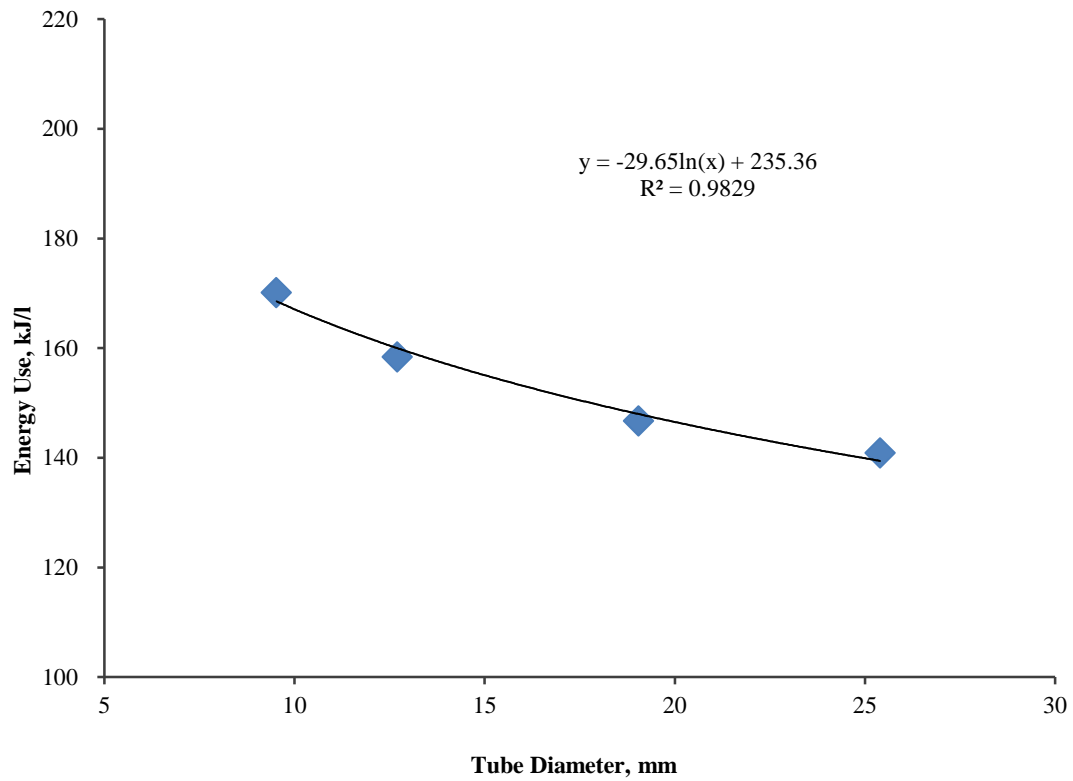


Figure 13 Energy use at increasing tube diameter

The minute temperature for all tube sizes is shown in Figure 11 below. On the other hand, the flat heating time is shown in the next figure (Figure 12).

Using the minute temperature plot, it shows that the product in the smallest tube (9.52 mm Ø) heats up 29× faster than the biggest tube (25.40 mm Ø). The product in the biggest tube is 2.67× bigger in terms of diameter and 19× bigger in terms of volume. As the tube gets bigger, the heating rate drops exponentially ($T_{t=60s} = -48\ln(x) + 183.65$, $R^2 = 0.9751$).

In terms of heating time to steady state, as the product diameter increases linearly by 2.67×, it increases by 7.5×, from 2.141 to 16.105 min. Moreover, by the same fashion of tube size increase, the total heat load increases by almost 16×, from 0.73 to 11.39 kJ. Considering that the volume increases by about 19×, the total energy use per unit volume of the product drops by 83% from 170.06 to 140.84 kJ l⁻¹. This relationship is shown visually in the figure below (Figure 13).

4 Conclusion and recommendations

Based from the results above, the following conclusions are made:

- (1) The thermal resistance of the stainless conduit to heating is very minimal compared to the coconut water product;
- (2) As the tube size increases, the heat capacity of the product increases (exponential) significantly more than the conduit (linear);
- (3) For all tube sizes, the heat flux, although initially dispersed, slows down relatively fast (57% drop within 40 s);
- (4) As the product gets bigger linearly by diameter and exponentially by volume, the heating rate drops logarithmically ($T_{t=60s} = -48\ln(x) + 183.65$);
- (5) The energy use per unit volume of the product decreases logarithmically ($Q_u = -29.65\ln x + 235.36$) as the tube diameter increases.

It is recommended to reconcile these with another fluid flow modeling and simulation for a more detailed guidance

in the subsequent fabrication of the tubular heat exchanger.

Without the cost of trial and error fabrication and experiments, these results are beneficial to designers and engineers in sizing of heaters, minimizing fouling and optimizing energy efficiency as well as pasteurizer processing capacity.

Acknowledgement

This study was conducted with financial and material support from the Engineering Research and Development for Technology (ERDT) program of the Department of Science and Technology (DOST), Philippines, De La Salle University (DLSU), Manila, Philippines and the Philippine Center for Postharvest Development and Mechanization (PHilMech), Nueva Ecija, Philippines.

References

- Aguiar, H. F., and J. A. W. Gut. 2014. Continuous HTST pasteurization of liquid foods with plate heat exchangers: Mathematical modeling and experimental validation using a time-temperature integrator. *Journal of Food Engineering*, Vol. 123, Issue Feb 2014: 78–86.
- Barbosa-Canovas, G. V., and A. Ibarz. 2003. *Unit Operations in Food Engineering*. United States: CRC Press LLC.
- Berk, Z. 2013. Heat and mass transfer. In *Food Process Engineering and Technology*, 2nd ed, Steve L. Taylor, editor, p. 690. USA: Academic Press, Elsevier Inc CA.
- Bonafoni, G., and R. Capata. 2015. Proposed design procedure of a helical coil heat exchanger for an orc energy recovery system for vehicular application. *Renewable and Sustainable Energy Reviews*, 80(October): 2412–5954.
- Dassault Systèmes SolidWorks Corporation. 2020. *Fundamentals of 3D Design and Simulation*. Available at: <https://www.solidworks.com/sites/default/files/2020-05/Fundamentals3DDesign-SIM-ENG-SV.pdf>. Accessed 12 April 2020.
- Fontan, R. da C. I., R. Cristina, F. Bonomo, A. R.Lemos, R. P. Ribeiro, and C. M. Veloso. 2007. Thermophysical properties of coconut water affected by temperature. *Journal of Food Process Engineering*, 32(2009): 382-397.

- Guan, X., and T. B. Martonen. 1997. Simulations of flow in curved tubes. *Aerosol Science and Technology*, 26(6): 485-504.
- Gutierrez, C. G. C. C., G. N. Diniz, and J. A. W. Gut. 2014. Dynamic simulation of a plate pasteurizer unit: Mathematical modeling and experimental validation. *Journal of Food Engineering*, 131(Jun): 124-134.
- Jha, A., J. A. Moses, and C. Anandharamakrishnan. 2019. Optimizing beverage pasteurization using computational fluid dynamics. In *Preservatives and Preservation Approaches in Beverages: The Science of Beverages*, vol. 15, issue September. Semantic Scholar, WA, USA.
- Kic, P., and M. Zajicek. 2015. CFD model of regenerative heat exchanger. *CIGR Journal*, 2015 (Special Issue, 18th World Congress, CIGR): 80–93.
- Listertube. 2020. *Tube bending design guide*. Available at: <https://www.listertube.com/links/tube-bending-design-guide/>. Accessed 2020 April 12.
- Mathisson, J. 2015. *Heat Exchangers. The Dairy Processing Handbook*. Available at: <https://www.tetrapak.com/about/tetra-pak-dairy-processing-handbook/>. Accessed 12 April 2020.
- Narataruksa, P., W. Pichitvittayakarn, P. J. Heggs, and S. Tia. 2010. Fouling behavior of coconut milk at pasteurization temperatures. *Applied Thermal Engineering*, 30(11–12): 1387–1395.
- Negiz, A., P. Ramanauskas, A. Qnar, J. E. Schlessler, and D. J. Armstrong. 1998. Modeling, monitoring and control strategies for high temperature short time Lethality-based control. *Food Control*, 9(1): 17-28.
- Petermeier, H., R. Benning, A. Delgado, U. Kulozik, J. Hinrichs, and T. Becker. 2002. Hybrid model of the fouling process in tubular heat exchangers for the dairy industry. *Journal of Food Engineering*, 55(1): 9-17.
- Petruzzi, L., D. Campaniello, B. Speranza, M. R. Corbo, M. Sinigaglia, and A. Bevilacqua. 2017. Thermal treatments for fruit and vegetable juices and beverages: A literature overview. *Comprehensive Reviews in Food Science and Food Safety*, 668–691. <https://onlinelibrary.wiley.com/doi/10.1111/1541-4337.12270>. Accessed 12 April 2020
- Shawyer, M., and A. F. M. Pizzali. 2003. Thermal Insulation Materials, Technical Characteristics And Selection Criteria. FAO Fisheries Technical Paper No. 436. Available at: <http://www.fao.org/3/y5013e/y5013e08.htm>. Accessed 11 October 2020.
- The World Material. 2020. Grade AISI SS316 Stainless Steel Properties. Material, The World. Available at: <https://www.theworldmaterial.com/aisi-316-ss316-stainless-steel-properties-composition/>. Accessed 11 May 2020.
- University of Guelph. 2020. Pasteurization. Food Science. Available at: <https://www.uoguelph.ca/foodscience/book/export/html/1898>. Accessed 11 October 2020.
- Welti-Chanes, J., F. Vergara-Balderas, and D. Bermúdez-Aguirre. 2005. Transport phenomena in food engineering: Basic concepts and advances. *Journal of Food Engineering*, 67(1–2): 113–128.